Direct Triple Annulations: A Way to Design Large Triazastarphenes with Intertwined Hexagonal Packing

published version: https://pubs.acs.org/doi/10.1021/acs.orglett.1c04001

Direct Triple Annulations: A Way to Design Large Triazastarphenes with Intertwined Hexagonal Packing

Qian Li, Chady Moussallem, Frédéric Castet, Luca Muccioli, Marie-Anne Dourges, Thierry Toupance,* and Yohann Nicolas*

Corresponding Authors
Thierry Toupance – *Univ. Bordeaux, CNRS, Bordeaux INP, ISM, UMR 5255, F-33405 Cedex Talence, France;* orcid.org/0000-0001-8234-7064; Email: thierry.toupance@u-bordeaux.fr
Yohann Nicolas – *Univ. Bordeaux, CNRS, Bordeaux INP, ISM, UMR 5255, F-33405 Cedex Talence, France;* orcid.org/0000-0003-3347-0431; Email: yohann.nicolas@enscbp.fr

Authors
Qian Li – *Univ. Bordeaux, CNRS, Bordeaux INP, ISM, UMR 5255, F-33405 Cedex Talence, France*
Chady Moussallem – *Univ. Bordeaux, CNRS, Bordeaux INP, ISM, UMR 5255, F-33405 Cedex Talence, France; Université Libanaise, Faculté des Sciences, Laboratoire de Chimie, Campus Michael Slayman, 1352 Rasmaska, Lebanon;* orcid.org/0000-0002-7325-9430
Frédéric Castet – *Univ. Bordeaux, CNRS, Bordeaux INP, ISM, UMR 5255, F-33405 Cedex Talence, France;* orcid.org/0000-0002-6622-2402
Luca Muccioli – *Department of Industrial Chemistry "Toso Montanari", University of Bologna, 40136 Bologna, Italy;* orcid.org/0000-0001-9227-1059
Marie-Anne Dourges – *Univ. Bordeaux, CNRS, Bordeaux INP, ISM, UMR 5255, F-33405 Cedex Talence, France*

ABSTRACT: A new straightforward synthetic strategy has been elaborated to achieve star-shaped triazatrinaphthylene and, for the *fi*rst time, triazatrianthrylene derivatives. Their solution- and solid- state properties were thoroughly characterized by cyclic voltammetry, UV–vis absorption spectroscopy, X-ray di*ff*raction, and density functional theory calculations. Original hexagonal molecular arrangements were found in the crystal phase, which opens a new pathway for designing materials with improved three-dimensional charge-transport properties.

Over the past two decades, π-conjugated materials have undergone new developments after the discovery of their conductive properties.[1] Most of these organic materials display anisotropic charge transport in the crystal phase, an imbalance that can be detrimental for speci*fi*c applications such as solid- state dye sensitized solar cells (SD-DSSCs), perovskite solar cells (PSCs), bulk heterojunction (BHJ), photovoltaic devices (OPVs), and organic light-emitting diodes (OLEDs).[2−4] Bulk materials exhibiting one-dimensional (1D) charge transport are particularly sensitive to spatial defects, contrary to materials with isotropic conductivity, owing to the availability for the latter of multiple charge percolation pathways.
In this context, fullerene (C60) is considered to be the "perfect" material owing to its spherical shape.[5,6] For the last 20 years, the performance of C60 derivatives for electron transport has been unrivaled in the field of BHJ solar cells,[7] in which 3D charge transport is required. However, a new class of molecules, broadly referred to as nonfullerene acceptors (NFAs), was recently reported to offer advantageous alternatives.[8−12] Most NFA chemical structures are distorted or bear bulky groups, often restricting their propensity to crystallize. Nonetheless, a crystal packing with efficient π- interactions is in general required for achieving high mobility.[13,14] Therefore, a compromise has to be made to

preserve π-stacking while avoiding anisotropic charge trans- port. In this context, a three-bladed rylene propeller-shaped material has shown both large 3D network intermolecular π- stacking in single crystals and high performances in OPV cells.[15] More generally, the design of molecules leading to 3D charge transport in the crystalline phase is a challenging and desired objective.[16]

In this paper, the design strategy has been inspired by John Anthony's research work on pentacene derivatives, where bulky groups enforce translations in the aromatic plane and a brick-wall arrangement, which improves the charge transport dimensionality into two directions.[17–20] With the objective of designing new 3D charge transport materials, we applied a similar design concept to star-shaped molecules with C_{3h} symmetry, as shown in Figure 1. The designed molecules consist of a planar trigonal core of fused aromatic cycles (referred to as "arms" in the following) and three bulky side groups located close to the center (referred to as the "branches"). In such molecular structures, π-conjugated arms are supposed to form efficient π-stacking with neighboring molecules while different branches with large steric hindrance are introduced to increase the solubility of the materials, to prevent 1D columnar packing, and to modulate π orbital overlaps.

On the basis of the designed molecular structure, two speculative supramolecular arrangements are depicted in Figure 1. First, molecules can pack either through intermo- lecular π-stacking along the arms (arm packing) or on top of each other (intertwined column packing) to form a first dimer. Then, replicating the dimers to construct larger aggregates, two packing modes emerge, involving face-to-face π-stacking between the original molecule and six neighbors in different directions to form hexagons.

In order to follow the laid down design rules, the star-shaped cores are made of triazatrinaphthylenes (TAN) and triazatrianthrylenes (TAA), while the solubilizing branches consist of phenyl derivatives or trialkylsilylacetylene groups (Scheme 1). In this architecture, the smaller size of nitrogen compared to the C–H of trianthrylene should limit the steric hindrance between arms and branches, preventing any torsion of the fused aromatic cores.[21–23]

With regard to the chemical synthesis of these compounds, it is worth noting that large TAAs have never been obtained, contrary to the acridine cores they contain. The latter are frequently found in biological and medicinal areas[24] as well as in building blocks for dyes, pigments, ligands, *fl*uorescent sensors, and OLED materials.[25–29] In order to keep all intermediates soluble during the synthetic process, we focused on reaction pathways in which ring closure arises as the last step. A synthetic route of acridine derivatives[30,31] was reported in two steps via Buchwald–Hartwig coupling,[32] and recently, a one-pot strategy was speci*fi*cally used for yielding acridine derivatives substituted by methoxy groups in positions 1 and 3.[33]

Consequently, the Buchwald–Hartwig coupling was first tested between the commercial 2-aminobenzophenone and 1,3,5-tribromobenzene (Scheme 1). Surprisingly, the final compound (TAN-Ph) was obtained in one step, showing that amination and cyclization occurred three times in one pot with a high yield, i.e., 66%. In order to understand the reaction mechanism and its limitations, reactions of 2-aminobenzophe- none were carried out with both bromobenzene and 1,4-dibromobenzene (Scheme S-A.3). In those cases, the reactions stopped after the *fi*rst aminations, proving that the aminations occurred before the annulations (Scheme S-A.5). In conclusion, the three substitutions on the 1,3,5 positions of a benzene by electron-releasing groups activate carbons to induce both cyclization and aromatization.

In order to lengthen the arms, this synthetic pathway was successfully extended to triazatrianthrylene derivatives without encountering solubility issues, which are frequently observed for large π-conjugated systems. Different phenyl substituents were easily introduced as branches (TAA-Ph, TAN-MePh, TAA-tBuPh, TAA-OMePh, TAA-CF_3Ph). However, when phenyl branches were substituted twice in the ortho positions, the cyclization steps did not occur (Scheme S-A.4). In addition, the versatility of this last one-step reaction was demonstrated with triple-bond substitutions as branches (TAA-Tips). Finally, seven new star-shaped molecules with different arm lengths and branch sizes were efficiently synthesized with a tandem reaction reaching up to 87% yield. All compounds were found to be thermally stable up to 400°C (Figure S–C.1), with the exception of TAA-Tips (362.5°C), while their actual C_{3h} symmetry in solution was evidenced by the single set of resonance for both arms in NMR spectra (Figures S–F).

UV–vis spectra of the seven compounds were recorded in dichloromethane (Figure 2). The spectra of TAN-Ph and TAN-MePh are very similar, with optical bandgaps estimated from the thresholds of the absorption spectra around 3.10 and 3.05 eV, respectively. These bandgaps are close to the values reported for 2,8,14-trimethyl-5,11,17-triazatrinaphthylene (TrisK-H-Me) in which the central starphene is not substituted.[34] These results indicate that electron conjugation does not extend over phenyl branches, as also evidenced by the electron density distribution of the frontier MOs (Figures S-E.1–7). This observation also holds true for the phenyl- substituted TAAs. As a consequence of their larger conjugated core, the maximum absorption band of the four TAA derivatives is red-shifted about 50 nm with respect to TAN derivatives, an effect which is quantitatively reproduced by DFT calculations. Interestingly, the UV–vis spectrum of TAA- Tips departs from the others, with a main absorption band red-shifted by an extra 20 nm. DFT calculations indicate that this shift arises from the conjugation between the triple bonds and the TAA core (Figure S-E.5). Finally, optical energy bandgaps lie far in the visible part of spectrum (2.38 eV for TAA-Tips and around 2.55 eV for the other).

To gain a deeper insight in the amplitude and dimensionality of charge transport within the six crystal structures, the electronic parameters characterizing the migration of charge carriers such as internal reorganization energies λ_i and transfer integrals J_{ij} in the hopping regime were evaluated at the B3LYP/6-31G(d) level (see the SI). For all compounds, internal reorganization energies for electron transport are remarkably low (below 0.1 eV), thus favoring the delocalization of the extra charge over multiple molecules. As discussed above, the nature of peripheral substituents has a strong impact on the molecular arrangement within the crystals, which translates into large variations in hole and electron transfer integrals (Table S-E.2). For TAN derivatives, TAA-tBuPh and TAA-TIPS, electronic couplings are negligible or display an alternation of nonequivalent dimers along one direction associated with high and low J_e values, which is detrimental for electron mobility.

Reversely, the overlap between the arms observed in TAA- OMePh (Figure 3) is at the origin of a network of π-stacking interactions associated with rather large electron transfer integrals and long distances and inscribed in a plane, clearly suggesting a 2D electron transport in this material. Finally, in the intertwined column packing (TAA-Ph), the maximum coupling is displayed for one dimer along the column direction (Figure 4). Moreover, nine secondary coupling terms ranging between 6 and 12 meV are also present

for long-range hopping (>15 Å), favoring intercolumnar charge transport pathways and then should help 3D percolation of the charges.

In conclusion, we reported a straightforward synthesis of star-shaped TAN by a tandem coupling-cyclization step. This synthetic strategy enabled reaching the extended TAA skeleton for the first time and, thus, designing large and soluble molecules with C_{3h} symmetry. A thorough investigation of their molecular properties through a combination of experimental and computational techniques demonstrated demonstrated that these materials are stable at ambient temperature and in their reduced states. Furthermore, single-crystal XRD analyses demonstrated that TAA-Ph and TAA-OMePh exhibit the originally speculated "intertwined column packing" and half "arm packing", both favorable for multidimensional charge transport. Electronic coupling terms calculated at the DFT level further support that TAA-OMePh and TAA-Ph could respectively exhibit 2D and 3D charge transport properties in the crystalline phase, a key feature for the realization of high-performance OSCs.

ACKNOWLEDGMENTS

Q.L. thanks the Chinese Scholarship Council for her PhD grant. Computer time was provided by the Pôle Modélisation HPC facilities of the Institut des Sciences Moléculaires, cofunded by the Nouvelle Aquitaine region, as well as by the MCIA (Mésocentre de Calcul Intensif Aquitain) resources of Université de Bordeaux and of Université de Pau et des Pays de l'Adour.

REFERENCES

(1) Paterson, A. F.; Singh, S.; Fallon, K. J.; Hodsden, T.; Han, Y.; Schroeder, B. C.; Bronstein, H.; Heeney, M.; McCulloch, I.; Anthopoulos, T. D. Recent Progress in High-Mobility Organic Transistors: A Reality Check. Adv. Mater. 2018, 30 (36), 1–33.

(2) Sawatzki, F. M.; Doan, D. H.; Kleemann, H.; Liero, M.; Glitzky, A.; Koprucki, T.; Leo, K. Balance of Horizontal and Vertical Charge Transport in Organic Field-Effect Transistors. Phys. Rev. Appl. 2018, 10 (3), 1.

(3) Park, S. K.; Kim, J. H.; Park, S. Y. Organic 2D Optoelectronic Crystals: Charge Transport, Emerging Functions, and Their Design Perspective. Adv. Mater. 2018, 30 (42), 1–26.

(4) Yin, X.; Song, Z.; Li, Z.; Tang, W. Toward Ideal Hole Transport Materials: A Review on Recent Progress in Dopant-Free Hole Transport Materials for Fabricating Efficient and Stable Perovskite Solar Cells. Energy Environ. Sci. 2020, 13 (11), 4057–4086.

(5) Tamura, H.; Tsukada, M. Role of Intermolecular Charge Delocalization on Electron Transport in Fullerene Aggregates. Phys. Rev. B: Condens. Matter Mater. Phys. 2012, 85 (5), 1–8.

(6) D'Avino, G.; Olivier, Y.; Muccioli, L.; Beljonne, D. Do Charges Delocalize over Multiple Molecules in Fullerene Derivatives? J. Mater. Chem. C 2016, 4 (17), 3747–3756.

(7) Acquah, S. F. A.; Penkova, A. V.; Markelov, D. A.; Semisalova, A. S.; Leonhardt, B. E.; Magi, J. M. Review The Beautiful Molecule: 30 Years of C 60 and Its Derivatives. ECS J. Solid State Sci. Technol. 2017, 6 (6), M3155–M3162.

(8) Lin, H.; Wang, Q. Non-Fullerene Small Molecule Electron Acceptors for High-Performance Organic Solar Cells. J. Energy Chem. 2018, 27 (4), 990–1016.

(9) Li, S.; Zhang, Z.; Shi, M.; Li, C. Z.; Chen, H. Molecular Electron Acceptors for Efficient Fullerene-Free Organic Solar Cells. Phys. Chem. Chem. Phys. 2017, 19 (5), 3440–3458.

(10) Li, H.; Earmme, T.; Ren, G.; Saeki, A.; Yoshikawa, S.; Murari, N. M.; Subramaniyan, S.; Crane, M. J.; Seki, S.; Jenekhe, S. A. Beyond Fullerenes: Design of Nonfullerene Acceptors for Efficient Organic Photovoltaics. J. Am. Chem. Soc. 2014, 136 (41), 14589–14597.

(11) Armin, A.; Li, W.; Sandberg, O. J.; Xiao, Z.; Ding, L.; Nelson, J.; Neher, D.; Vandewal, K.; Shoaee, S.; Wang, T.; Ade, H.; Heumüller, T.; Brabec, C.; Meredith, P. A History and Perspective of Non- Fullerene Electron Acceptors for Organic Solar Cells. Adv. Energy Mater. 2021, 11 (15), 1–42.
(12) Yue, Q.; Liu, W.; Zhu, X. N-Type Molecular Photovoltaic Materials: Design Strategies and Device Applications. J. Am. Chem. Soc. 2020, 142 (27), 11613–11628.
(13) Li, A.; Yan, L.; He, C.; Zhu, Y.; Zhang, D.; Murtaza, I.; Meng, H.; Goto, O. In-Plane Isotropic Charge Transport Characteristics of Single-Crystal FETs with High Mobility Based on 2,6-Bis(4-Methoxyphenyl)Anthracene: Experimental Cum Theoretical Assess- ment. J. Mater. Chem. C 2017, 5 (2), 370–375.
(14) Takimiya, K.; Nakano, M.; Sugino, H.; Osaka, I. Design and Elaboration of Organic Molecules for High Field-Effect-Mobility Semiconductors. Synth. Met. 2016, 217, 68–78.
(15) Meng, D.; Fu, H.; Xiao, C.; Meng, X.; Winands, T.; Ma, W.; Wei, W.; Fan, B.; Huo, L.; Doltsinis, N. L.; Li, Y.; Sun, Y.; Wang, Z. Three-Bladed Rylene Propellers with Three-Dimensional Network Assembly for Organic Electronics. J. Am. Chem. Soc. 2016, 138 (32), 10184–10190.
(16) Skabara, P. J.; Arlin, J. B.; Geerts, Y. H. Close Encounters of the 3D Kind - Exploiting High Dimensionality in Molecular Semi- conductors. Adv. Mater. 2013, 25 (13), 1948–1954.
(17) Anthony, J. E.; Brooks, J. S.; Eaton, D. L.; Parkin, S. R. Functionalized Pentacene: Improved Electronic Properties from Control of Solid-State Order. J. Am. Chem. Soc. 2001, 123 (38), 9482–9483.
(18) Gruntz, G.; Lee, H.; Hirsch, L.; Castet, F.; Toupance, T.; Briseno, A. L.; Nicolas, Y. Nitrile Substitution Effect on Triphenodioxazine-Based Materials for Liquid-Processed Air-Stable n-Type Organic Field Effect Transistors. Adv. Electron. Mater. 2015, 1 (6), No. 1500072, (1–6).
(19) Zhang, L.; Cao, Y.; Colella, N. S.; Liang, Y.; Brédas, J. L.; Houk, K. N.; Briseno, A. L. Unconventional, Chemically Stable, and Soluble Two-Dimensional Angular Polycyclic Aromatic Hydrocarbons: From Molecular Design to Device Applications. Acc. Chem. Res. 2015, 48 (3), 500–509.
(20) Xu, X.; Yao, Y.; Shan, B.; Gu, X.; Liu, D.; Liu, J.; Xu, J.; Zhao, N.; Hu, W.; Miao, Q. Electron Mobility Exceeding 10 Cm2V–1s– 1and Band-Like Charge Transport in Solution-Processed n-Channel Organic Thin-Film Transistors. Adv. Mater. 2016, 28 (26), 5276– 5283.
(21) Saris, P. J. G.; Thompson, M. E. Gram Scale Synthesis of Benzophenanthroline and Its Blue Phosphorescent Platinum Com- plex. Org. Lett. 2016, 18 (16), 3960–3963.
(22) Ahmed, F. R.; Trotter, J. The Crystal Structure of Triphenylene. Acta Crystallogr. 1963, 16 (6), 503–508.
(23) Simhai, N.; Iverson, C. N.; Edelbach, B. L.; Jones, W. D. Formation of Phenylene Oligomers Using Platinum-Phosphine Complexes. Organometallics 2001, 20 (13), 2759–2766.
(24) Prasher, P.; Sharma, M. Medicinal Chemistry of Acridine and Its Analogues. MedChemComm 2018, 9 (10), 1589–1618.
(25) Olmsted, J. Calorimetric Determinations of Absolute Fluorescence Quantum Yields. J. Phys. Chem. 1979, 83 (20), 2581– 2584.
(26) Chemistry of Heterocyclic Compounds: A Series Of Monographs; Acheson, R. M., Ed.; John Wiley & Sons, Inc.: Hoboken, 1973.
(27) Gunanathan, C.; Milstein, D. Metal-Ligand Cooperation by Aromatization-Dearomatization: A New Paradigm in Bond Activation and “Green” Catalysis. Acc. Chem. Res. 2011, 44 (8), 588–602.
(28) Yang, Y. K.; Tae, J. Acridinium Salt Based Fluorescent and Colorimetric Chemosensor for the Detection of Cyanide in Water. Org. Lett. 2006, 8 (25), 5721–5723.
(29) Ding, L.; Dong, S. C.; Jiang, Z. Q.; Chen, H.; Liao, L. S. Orthogonal Molecular Structure for Better Host Material in Blue Phosphorescence and Larger OLED White Lighting Panel. Adv. Funct. Mater. 2015, 25 (4), 645–650.
(30) Schmidt, A.; Liu, M. Recent Advances in the Chemistry of Acridines. In Advances in Heterocyclic Chemistry; Elsevier, 2015; Vol. 115, pp 287–353.
(31) Brikci-Nigassa, N. M.; Bentabed-Ababsa, G.; Erb, W.; Chevallier, F.; Picot, L.; Vitek, L.; Fleury, A.; Thiéry, V.; Souab, M.; Robert, T.; Ruchaud, S.; Bach, S.; Roisnel, T.; Mongin, F. 2- Aminophenones, a Common Precursor to N-Aryl Isatins and Acridines Endowed with Bioactivities. Tetrahedron 2018, 74 (15), 1785–1801.

(32) Tsvelikhovsky, D.; Buchwald, S. L. Synthesis of Heterocycles via Pd-Ligand Controlled Cyclization of 2-Chloro-N-(2-Vinyl)- Aniline: Preparation of Carbazoles, Indoles, Dibenzazepines, and Acridines. J. Am. Chem. Soc. 2010, 132 (40), 14048−14051.
(33) Wang, T. J.; Chen, W. W.; Li, Y.; Xu, M. H. Facile Synthesis of Acridines via Pd(0)-Diphosphine Complex-Catalyzed Tandem Coupling/Cyclization Protocol. Org. Biomol. Chem. 2015, 13 (23), 6580−6586.
(34) Bertrand, H.; Guillot, R.; Teulade-Fichou, M. P.; Fichou, D. Synthesis, Properties, and Remarkable 2D Self-Assembly at the Liquid/Solid Interface of a Series of Triskele-Shaped 5,11,17-Triazatrinaphthylenes (TrisK). Chem. - Eur. J. 2013, 19 (43), 14654−14664.
(35) Méndez-Hernández, D. D.; Tarakeshwar, P.; Gust, D.; Moore, T. A.; Moore, A. L.; Mujica, V. Simple and Accurate Correlation of Experimental Redox Potentials and DFT-Calculated HOMO/LUMO Energies of Polycyclic Aromatic Hydrocarbons. J. Mol. Model. 2013, 19 (7), 2845−2848.

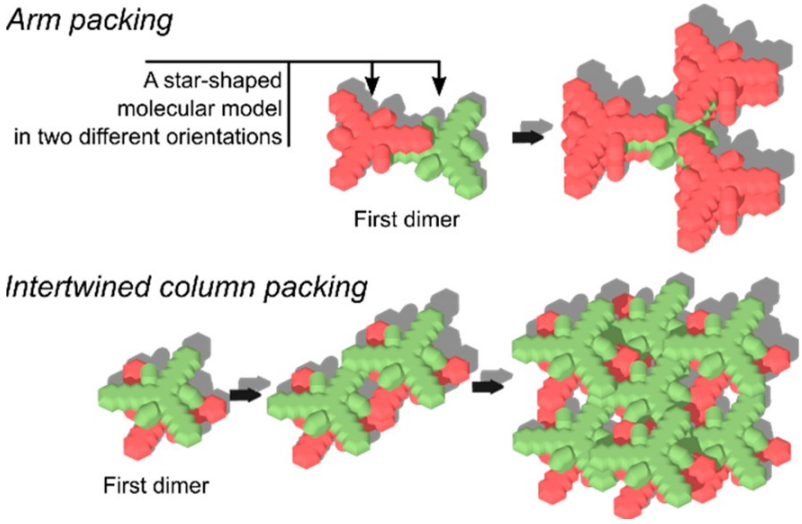

Figure 1. Representative views of possible molecular arrangements.

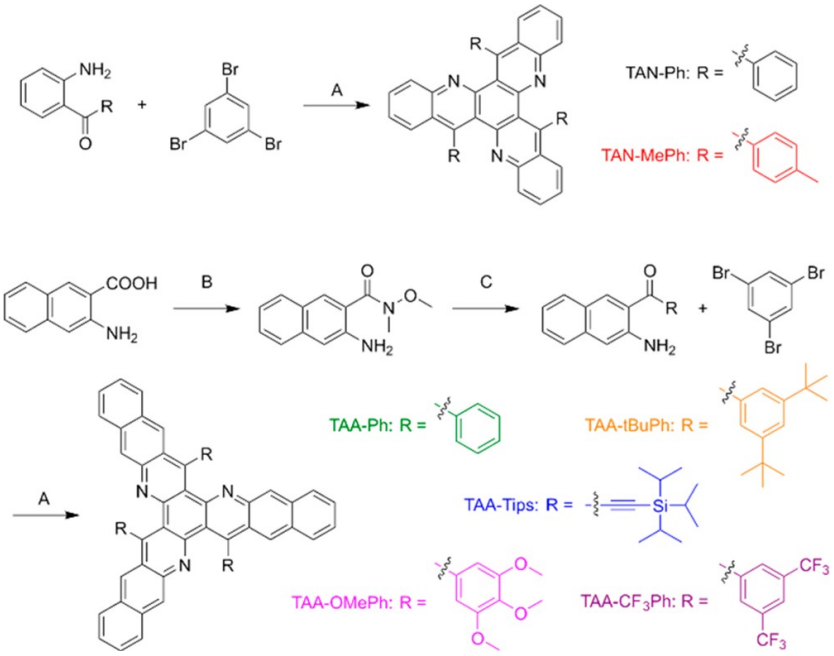

Scheme 1. Synthetic Routes toward TANs and TAAs[a]

[a]Key: (A) $Pd_2(dba)_3$, Brettphos, K_2CO_3, *t*-BuOH, 100 °C, 24 h; (B) MeNHOMe·HCl, DPCP, Et_3N, DCM, 0 °C overnight; (C) Br-R or H-R, *n*-BuLi, THF, −78 °C or PhMgCl, THF, 0 °C.

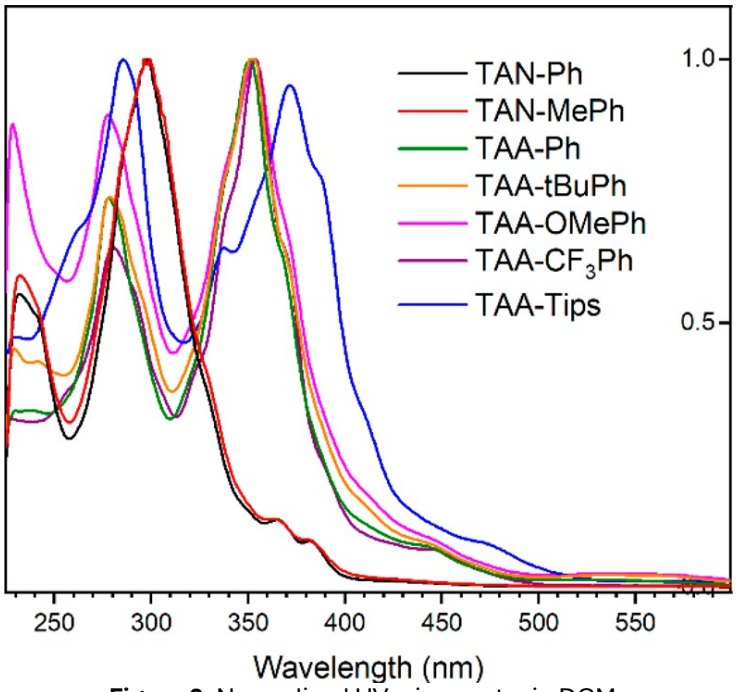

Figure 2. Normalized UV–vis spectra in DCM.

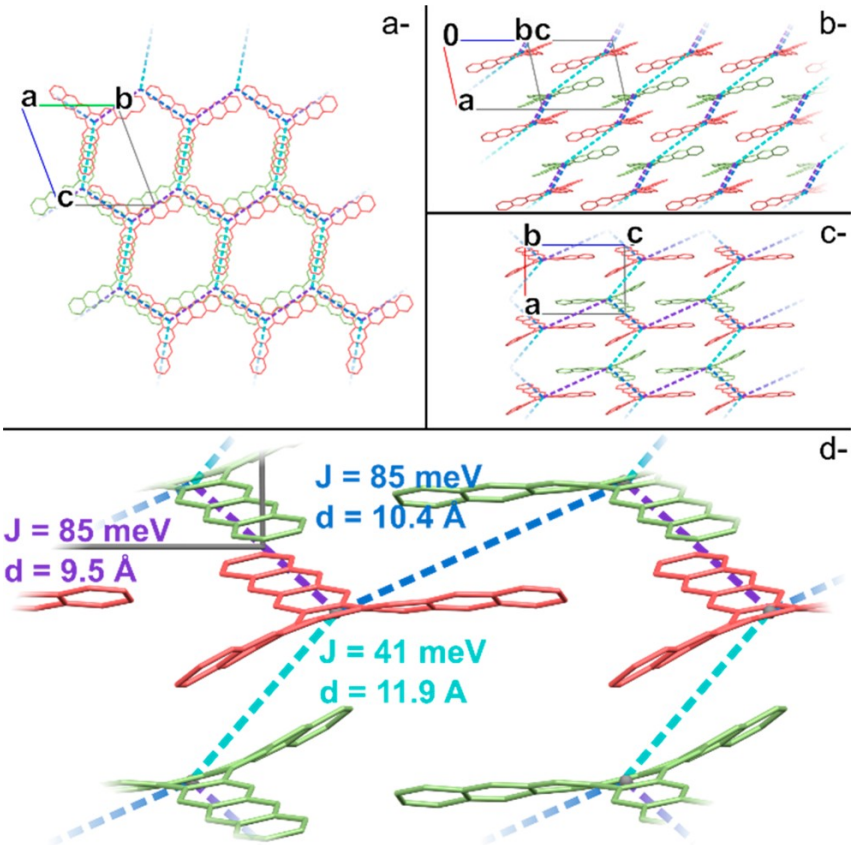

Figure 3. Molecular packing and charge transport pathways (dotted line) for TAA-OMePh (a, view normal to [100] plane; b, to [0$\bar{1}$1]; c, to [010]; d, zoom of c view). For the sake of clarity, hydrogen atoms and lateral branches have been omitted. *d* is the distance between two neighboring molecules (in Å). *J* is the calculated electronic coupling related to electron transport (in meV).

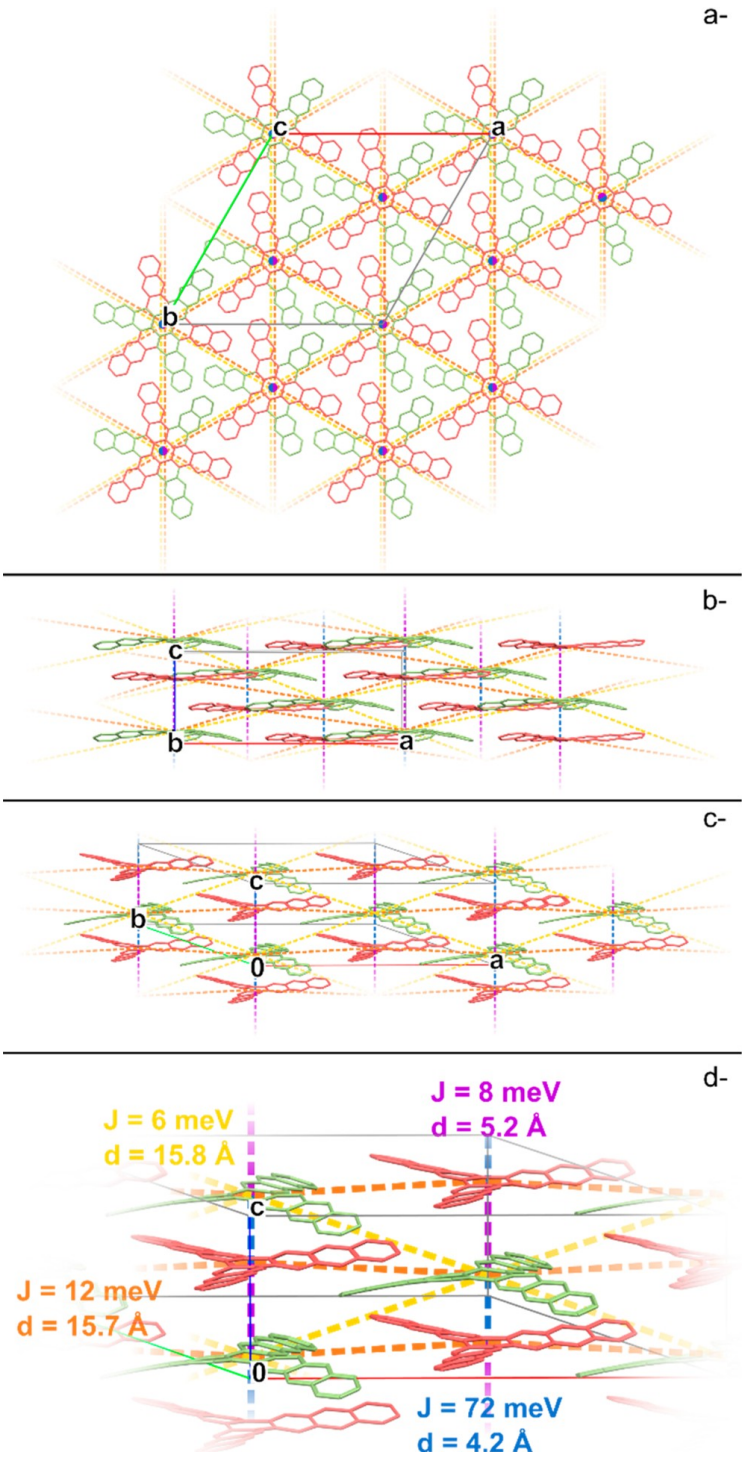

Figure 4. Molecule packing and charge transport pathways (dotted line) for TAA-Ph (a, view normal to [001] plane; b, to [010], c, to [12$\bar{1}$]; d, zoom of c view). For the sake of clarity, hydrogen atoms and lateral branches have been omitted. *d* is the distance between two neighboring molecules (in Å). *J* is the calculated electronic coupling related to electron transport (in meV).